Sensor and Simulation Notes

Note 358

June 1993

# The Radiation Pattern of Reflector Impulse Radiating Antennas:
## Early-Time Response

Everett G. Farr
Farr Research
Albuquerque, NM 87123

Carl E. Baum
Phillips Laboratory
Kirtland AFB, NM 87117

## Abstract

We generate here an approximation to the step response of reflector Impulse Radiating Antennas (IRAs) in the E- and H-planes. These step responses are then convolved with the derivative of the driving voltage to find the radiated fields. This allows a determination of the radiation pattern of reflector IRAs.

# I. Introduction

The transient radiation from a planar aperture field distribution was developed in [1]. This was further specialized to two-wire apertures in [2], but only on boresight. The off-boresight fields created by a two-wire aperture were never developed. We do so in this paper.

The results we provide here are valid for a wide variety of practical cases. Although it is true that these results are valid only at high impedances, this is not very confining in practice, because at low impedances one incurs significant feed blockage anyway. Furthermore, our expressions are derived explicitly only for round wire feeds. But since the feed arms are relatively thin at high impedances, the specific shape of the feed should not matter very much. Thus, the results developed here are useful for other feed arm shapes, such as coplanar plates and curved plates [3].

We begin by providing a review of the static fields between two wires. This is the field we find in the aperture of a reflector IRA. Next, we radiate this field with a step-function driving voltage. Expressions are provided for the E-plane and H-plane fields (pattern) created when the aperture fields are turned on suddenly. Furthermore, we demonstrate that on boresight our results are consistent with earlier results calculated by contour integration. Finally, we convolve the step response with the derivative of a typical driving voltage, in order to get the response to a realistic driving voltage. With this information, we can calculate a gain and antenna pattern, according to the definitions of [4].

## II.    Static Fields in the Two-Wire Aperture

Let us review first the static fields in a two-wire aperture. We assume a Reflector IRA with a relatively high feed impedance, so we can ignore aperture blockage for early times. We can estimate the error incurred by ignoring aperture blockage from [3].

Recall that the effect of the paraboloidal reflector is to convert a spherical TEM wave into a (locally) planar TEM wave [5, Appendix A]. Thus, we must radiate an aperture field that turns on suddenly, as shown in Figure 1. We assume the tangential aperture field has the form

$$E_t(x,y,t) = E_{t_x} - jE_{t_y} = -\frac{V}{\Delta u}\frac{dw(\zeta)}{d\zeta} u(t) \tag{2.1}$$

where $V$ is the voltage between the two wires, $u(t)$ is the Heaviside step function, and $w(\zeta)$ is the complex potential between the two wires described by

$$
\begin{aligned}
w(\zeta) &= u(\zeta) + jv(\zeta) \\
\zeta &= x + jy \\
u(\zeta) \,\&\, v(\zeta) &= \text{real functions}
\end{aligned}
\tag{2.2}
$$

Furthermore, we restrict ourselves to round wires, which makes the math considerably simpler. For this case, the potential function is [6]

$$w(\zeta) = 2j\operatorname{arccot}(\zeta/a) = \ln\left(\frac{\zeta-ja}{\zeta+ja}\right) \tag{2.3}$$

where $a$ is the aperture radius. This potential function is plotted in Figure 2. The real and imaginary parts of the potential can be separated as [10]

$$
\begin{aligned}
u(\zeta) &= \frac{1}{2}\ln\left[\frac{x^2+(a+y)^2}{x^2+(a-y)^2}\right] \\[2mm]
v(\zeta) &= \arctan\left[\frac{2x}{x^2+y^2-a^2}\right]
\end{aligned}
\tag{2.4}
$$

Finally, the impedance is

$$f_g = \frac{\Delta u}{\Delta v} \tag{2.5}$$

where $\Delta u$ is the change in $u$ from one conductor to the other, and $\Delta v$ is the change in $v$ as one encircles a conductor (in this case $2\pi$).
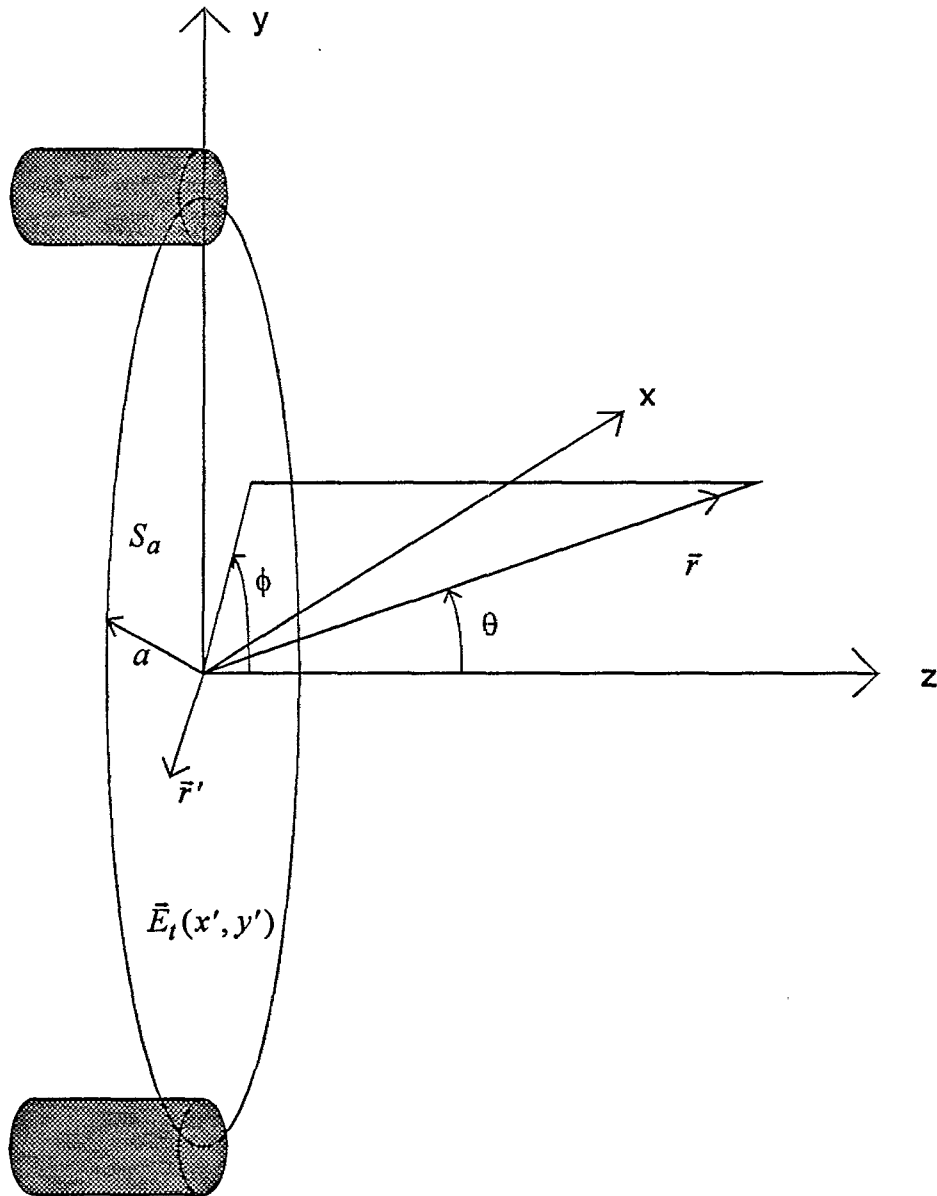
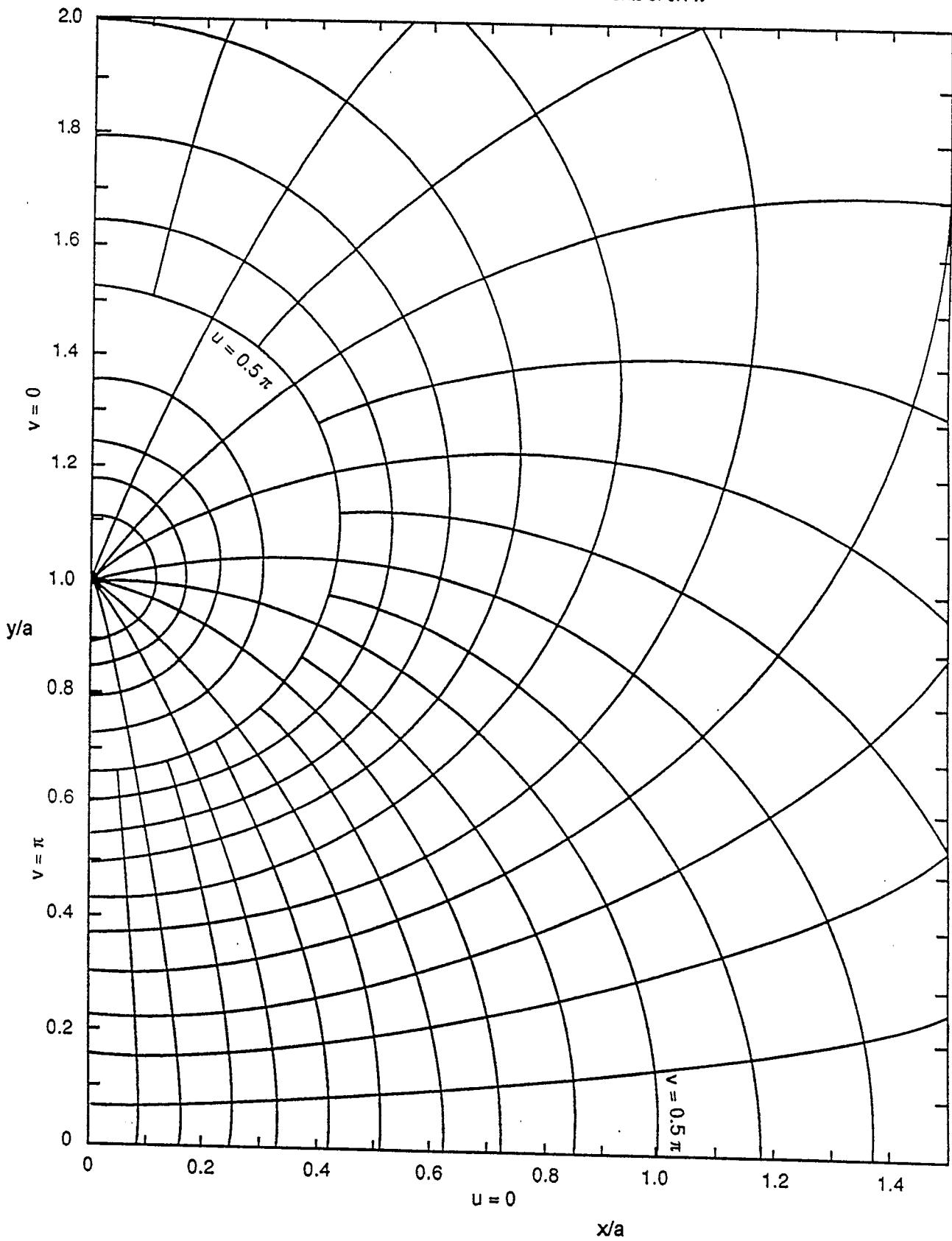Figure 1. The aperture field to be radiated.

Figure 2.  The complex potential map for round wires, upper right quadrant, from [2].

So far, this theory has just been a review. But in looking ahead, we know that certain additional functions will be of use to us later. Thus, let us define the following normalized potential function.

$$\Phi^{(h)}(x) = \frac{-1}{V} \int_{C_1(x)} E_y \, dy \qquad (2.6)$$

where the contour $C_1(x)$ is a vertical line through the point $(x,0)$ for the length of the circular aperture (Figure 3). We will see later that the radiated field in the H-plane is proportional to the above integral. As time progresses, the field will be proportional to $\Phi^{(h)}(x)$ as the contour $C_1(x)$ sweeps across the aperture. To simplify this integral, we use a standard formula for the $y$ component of the electric field,

$$E_y = -\frac{V}{\Delta u} \frac{\partial u(x,y)}{\partial y} \qquad (2.7)$$

where $u(\zeta)$ is defined in (2.4). Thus, we have

$$\Phi^{(h)}(x) = \frac{1}{\Delta u} \int_{C_1(x)} \frac{\partial u}{\partial y} \, dy = \frac{2}{\Delta u} u\left(x, \sqrt{a^2 - x^2}\right) \qquad (2.8)$$

This is just the relative change in $u$ along the path $C_1(x)$. When $C_1$ cuts through the metal conductor, the relative change in $u$ is unity. To the left and right of the conductor, the change in $u$ tapers off, reaching zero at the edge of the aperture. Using (2.4), after some simplification we find

$$\Phi^{(h)}(x) = \begin{cases} 1/(\pi f_g) \, \text{arcsech}(-x/a) & -a \leq x \leq -a \, \text{sech}(\pi f_g) \\ 1 & -a \, \text{sech}(\pi f_g) \leq x \leq a \, \text{sech}(\pi f_g) \\ 1/(\pi f_g) \, \text{arcsech}(x/a) & a \, \text{sech}(\pi f_g) \leq x \leq a \end{cases} \qquad (2.9)$$

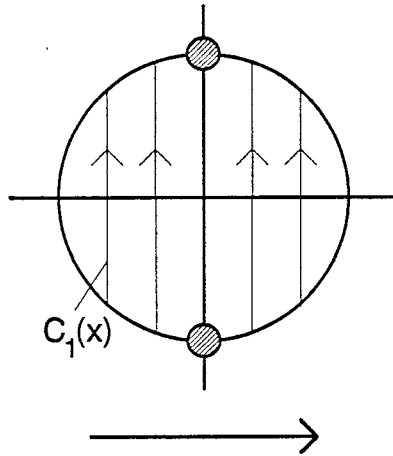This is plotted in Figure 4 for several values of $f_g$.
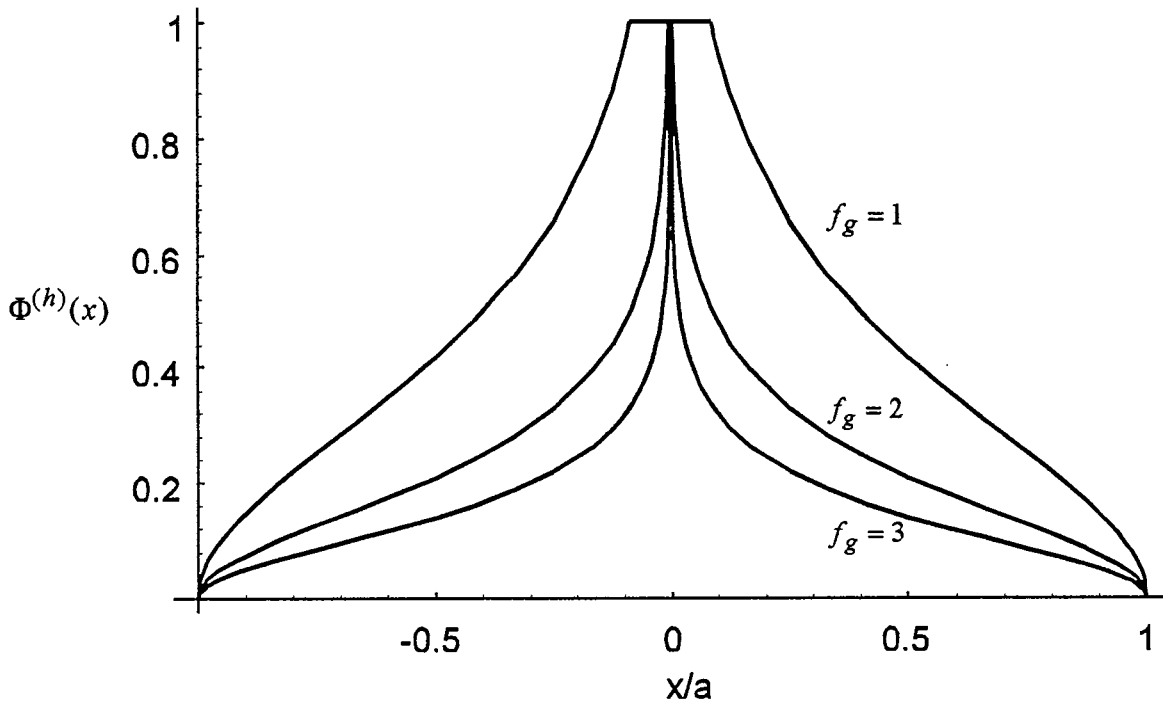
6

Figure 3. Location of $C_1(x)$.



Figure 4. Plots of $\Phi^{(h)}(x)$ as a function of $x/a$ and $f_g$.

There is a similar function we can define which is useful for a pattern cut in the E-plane. We will see later that the field in the E-plane is proportional to the line integral

$$\Phi^{(e)}(y) = \frac{-1}{V}\int_{C_2(y)} E_y \, dx \qquad (2.10)$$

7

where $C_2(y)$ is a horizontal line through the point $(0, y)$, for the length of the circular aperture (Figure 5). The field in the E-plane is proportional to the above integral as $C_2(y)$ sweeps across the aperture. We now write the usual expression for $E_y$, and convert to a derivative with respect to $x$ with the Cauchy-Riemann equations [9]. Thus, we have

$$E_y = -\frac{V}{\Delta u}\frac{\partial u}{\partial y} = \frac{V}{\Delta u}\frac{\partial v}{\partial x} \qquad (2.11)$$

Combining the above two equations, we find

$$\Phi^{(e)}(y) = \frac{-1}{\Delta u}\int_{C_2(y)}\frac{\partial v}{\partial x}dx = \frac{-2}{\Delta u}\left[v\left(\sqrt{a^2-y^2},y\right) - v(0,y)\right] \qquad (2.12)$$

We can simplify the above by noticing that for almost all values of $y$, the expression in square brackets is $-\Delta v/4$. If $C_2(y)$ intersects one of the wires, there is a small deviation from this simple result. But at high impedances the error is negligible because the wires are small. Thus, we have

$$\Phi^{(e)}(y) = \begin{cases} 1/(2f_g) & |y|\le a \\ 0 & \text{else} \end{cases} \qquad (2.13)$$

This is just a pulse function of width $a$ and magnitude $1/(2f_g)$. Another way of expressing this is

$$\Phi^{(e)}(y) = \frac{1}{2f_g}P(y,a) \qquad (2.14)$$

where $P(y,a)$ is a pulse function of value unity for $|y| \le a$ and zero elsewhere.

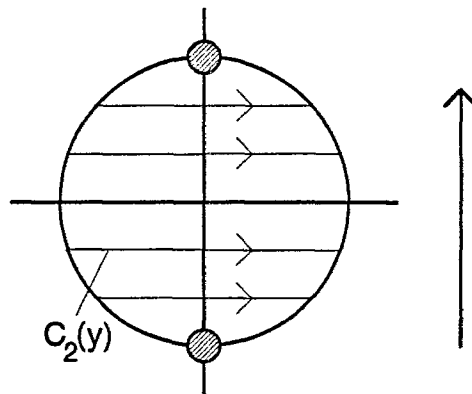This completes the review of the static fields in the aperture. Next, we apply this theory to the radiated field.



Figure 5. Location of $C_2(y)$.

## III. The Radiated Field

In [1] a general expression for the radiated far field generated by an arbitrary aperture field was derived. We now wish to specialize that expression to the field resulting from the aperture field between two wires.

Let us first provide some definitions.

$$
\begin{aligned}
s &= \text{Laplace Transform variable} \\
\gamma &= s/c \\
c &= \text{speed of light} \\
\bar{\bar{1}} &= \bar{1}_x \bar{1}_x + \bar{1}_y \bar{1}_y + \bar{1}_z \bar{1}_z \\
\bar{\bar{1}}_z &= \bar{\bar{1}} - \bar{1}_z \bar{1}_z = \bar{1}_y \bar{1}_y + \bar{1}_z \bar{1}_z
\end{aligned}
\tag{3.1}
$$

Furthermore, we define the tangential aperture field as

$$
\begin{aligned}
\bar{E}_t(x',y',t) &= \left[ \bar{1}_x E_x(x',y') + \bar{1}_y E_y(x',y') \right] u(t) \\
&= E_o \left[ \bar{1}_x g_x(x',y') + \bar{1}_y g_y(x',y') \right] u(t) \\
&= E_o \, \bar{g}(x',y') \, u(t)
\end{aligned}
\tag{3.2}
$$

where $E_o$ is the field at the center of the aperture. The radiated far field is now [1]

$$
\begin{aligned}
\bar{E}(\bar{r},s) &= e^{-\gamma r} \frac{E_o A}{2\pi c r} \tilde{\bar{F}}(\bar{1}_r, s) \\
\tilde{\bar{F}}(\bar{1}_r, s) &= \frac{1}{A} \left[ (\bar{\bar{1}}_z \cdot \bar{1}_r) \bar{\bar{1}} - (\bar{1}_z \bar{1}_r) \right] \cdot \int_{S_a} e^{\gamma(\bar{1}_r \cdot \bar{r}')} \bar{g}(x',y') \, dS'
\end{aligned}
\tag{3.3}
$$

where we have assumed a step-function time dependence of the driving voltage. To get the result for arbitrary time dependence, one would convolve the step response with the derivative of the driving voltage.

It can be shown from symmetry arguments [7] that the radiated field in the dominant planes (E-plane and H-plane) can be represented by just the dominant polarization, without a secondary or crosspol component. Another way of saying this is that it is only $E_y$ in the aperture that contributes to the radiated far field in the two major plane cuts. If we now specialize the above relationship to include just $E_y$, we have in the principal planes

9

$$\vec{E}(\vec{r},s) = e^{-\gamma r}\frac{E_o A}{2\pi c r}\tilde{\vec{F}}(\vec{1}_r,s)$$

$$\tilde{\vec{F}}(\vec{1}_r,s) = \left[\vec{1}_r \times \vec{1}_x\right]\tilde{f}_a(\vec{1}_r,s)$$

$$= \left[\sin(\phi)\vec{1}_\theta + \cos(\theta)\cos(\phi)\vec{1}_\phi\right]\tilde{f}_a(\vec{1}_r,s) \qquad (3.4)$$

$$\tilde{f}_a(\vec{1}_r,s) = \frac{1}{A}\int_{S_a} e^{\gamma(\vec{1}_r\cdot\vec{r}')}g_y(x',y')\,dS'$$

This is the expression we integrate over to get the field for the dominant polarization. Note that we have used the vector expression

$$\vec{A}\times(\vec{B}\times\vec{C}) = (\vec{A}\cdot\vec{C})\vec{B} - (\vec{A}\cdot\vec{B})\vec{C} \qquad (3.5)$$

to get the result in (3.4).

Let us simplify further (3.4), which is the complete radiated far field in one of the principal planes. The $y$ component of the aperture electric field can be expressed in various ways as

$$E_{t_y}(x',y') = E_o\,g_y(x',y') = -\frac{V}{\Delta u}\frac{\partial u}{\partial y} \qquad (3.7)$$

so the function $g_y$ is

$$g_y(x',y') = -\frac{V}{E_o\,\Delta u}\frac{\partial u(x,y)}{\partial y} \qquad (3.8)$$

The function $\tilde{f}_a(\vec{1}_r,s)$ in (3.4) now simplifies to

$$\tilde{f}_a(\vec{1}_r,s) = -\frac{V}{AE_o\,\Delta u}\int_{S_a} e^{\gamma(\vec{1}_r\cdot\vec{r}')}\frac{\partial u(x',y')}{\partial y'}\,dS' \qquad (3.9)$$

Converting to the time domain, we find

$$f_a(\vec{1}_r,t) = -\frac{V}{AE_o\,\Delta u}\int_{S_a}\frac{\partial u(x',y')}{\partial y'}\delta(t+\vec{1}_r\cdot\vec{r}'/c)\,dS' \qquad (3.10)$$

This is the result we must evaluate in both the E- and H-planes.

10

In the H-plane, where $\phi = 0$ or $\pi$, the function $f_a(\bar{1}_r, t)$ simplifies to

$$f_a^{(h)}(\theta, t) = -\frac{V}{AE_o \,\Delta u} \frac{c}{\sin(\theta)} \int_{C_a(x)} \frac{\partial u(ct/\sin(\theta), y')}{\partial y'} dy'$$

$$= -\frac{V}{AE_o} \frac{c}{\sin(\theta)} \Phi^{(h)}(ct/\sin(\theta)) \tag{3.11}$$

where we have used the function $\Phi^{(h)}(x)$ as defined in Section II. The superscript $h$ indicates that the expression is specialized to the H-plane. Combining this with (3.4), and noting that $\phi = 0$ or $\pi$ in the H-plane, we find

$$\boxed{\vec{E}^{(h)}(r, t) = \bar{1}_y \left( \frac{-V}{r} \right) \frac{\cot(\theta)}{2\pi} \Phi^{(h)}\left( \frac{ct}{\sin(\theta)} \right)} \tag{3.12}$$

Recall that in the H-plane, $\bar{1}_y = \pm \bar{1}_\phi$, where the "+" sign applies if $\phi = 0$ and the "-" sign applies for $\phi = \pi$. This is the final expression we need for the field in the H-plane. Note that we have normalized out a time delay of $r/c$, to keep the expression simple.

We can now plot some examples of these fields (Figure 6). If we normalize the time scale properly, the step response is dependent solely upon $f_g$ and $\theta$. Thus, it is convenient to normalize the time scale to $t_a = a/c$.
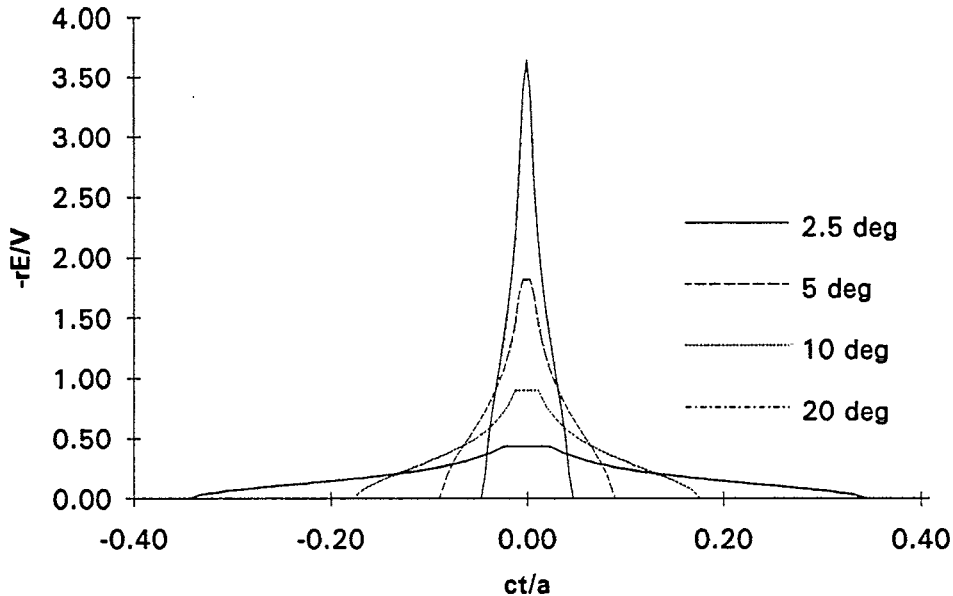


Figure 6. H-plane step response, for various values of $\theta$. For these plots, $Z_c = 400\,\Omega$ ($f_g = 1.0631$).

11

We can find similar expressions now for the E-plane. Proceeding from (3.10), and confining ourselves to the E-plane, where $\phi = \pi/2$ or $3\pi/2$, we find

$$f_a^{(e)}(\theta,t) = -\frac{V}{AE_o \, \Delta u} \frac{c}{\sin(\theta)} \int_{C_2(y)} \frac{\partial u(x',ct/\sin(\theta))}{\partial y'} \, dx'$$

$$= \frac{V}{AE_o \, \Delta u} \frac{c}{\sin(\theta)} \int_{C_2(y)} \frac{\partial v(x',ct/\sin(\theta))}{\partial x'} \, dx'$$

(3.13)

Expressing this in terms of the normalized potential function for the E-plane, $\Phi^{(e)}(y)$, we find

$$f_a^{(e)}(\theta,t) = -\frac{V}{AE_o} \frac{c}{\sin(\theta)} \Phi^{(e)}(ct/\sin(\theta))$$

$$= -\frac{V}{AE_o} \frac{c}{\sin(\theta)} \frac{1}{2f_g} P(x,a)$$

(3.14)

where $P(x,a)$ is the pulse function described in Section II. Combining this with (3.4), and noting that $\phi = \pi/2$ or $3\pi/2$ in the E-plane, we have

$$\boxed{\begin{aligned} \bar{E}^{(e)}(r,\theta,t) &= \pm \bar{1}_\theta \left(\frac{-V}{r}\right) \frac{1}{2\pi\sin(\theta)} \, \Phi^{(e)}\left(\frac{ct}{\sin(\theta)}\right) \\ &= \pm \bar{1}_\theta \left(\frac{-V}{r}\right) \frac{1}{4\pi f_g \sin(\theta)} \, P\left(\frac{ct}{\sin(\theta)},a\right) \end{aligned}}$$

(3.15)

where the "+" applies if $\phi = \pi/2$, and the "-" sign applies if $\phi = 3\pi/2$. This is the final expression for the field in the E-plane due to the $y$ component of the aperture field. Some examples of these fields are plotted in Figure 7.
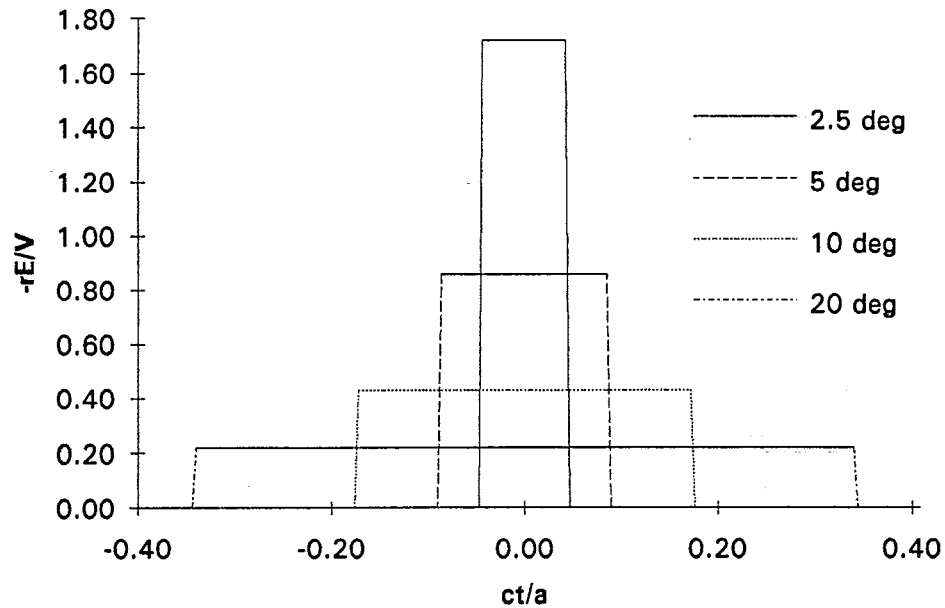
Figure 7.  E-plane  step  response,  for  various  values  of  $\theta$.   For  these  plots,  $Z_c = 400\ \Omega$ ($f_g = 1.0631$).


Let us review now the approximations we have used.  We have ignored aperture blockage, which limits us to higher feed impedances.  We have also ignored some of the fine detail in the E-plane step response that occurs close to the wires.  This has the effect of making the E-plane step response a slightly sharper pulse function than it actually is.  We have not invoked any small-angle approximations, however, so our expressions should be approximately valid out to $\theta = 90^\circ$.

We now have the step response in the E- and H-planes of an IRA in equations (3.12) and (3.15).  Before going further, we check that our two expressions provide the correct result on boresight.

## IV. Consistency Check on Boresight

We need to check that the expressions we have just developed for the H-plane and E-plane fields generate the correct results on boresight. Recall that the high-impedance approximation on boresight calculated by contour integration is [2]

$$E(r,t) = \frac{-V}{r}\frac{a}{2\pi c f_g}\,\delta_a(t) \tag{4.1}$$

where $\delta_a(t)$ is the approximate delta function [1], which converges to a true delta function in the limit as $r \to \infty$. Thus, the expressions for the E-plane and H-plane fields must approach this answer at $\theta = 0$, and at high impedances. Since it is simplest to show this for the E-plane result, we do this first.

The E-plane expression for the field on boresight is

$$\bar{E}^{(e)}(r,\theta,t) = \pm \bar{1}_\theta \left(\frac{-V}{r}\right)\frac{1}{4\pi f_g \sin(\theta)}\,P\left(\frac{ct}{\sin(\theta)},a\right) \tag{4.2}$$

In comparing (4.1) and (4.2), we find that if the two expressions are equivalent on boresight, then the following must also be true

$$\delta(t) = \lim_{\theta \to 0}\frac{c}{2a\sin(\theta)}\,P\left(\frac{ct}{\sin(\theta)},a\right) \tag{4.3}$$

Recall now the characteristics of a function that make it a $\delta$ function. First, the value of the function must approach infinity at $t = 0$. For the above function, this is obviously true. Second, the integral of the function (area) must be unity. Integrating (4.3), we find

$$\lim_{\theta \to 0}\frac{c}{2a\sin(\theta)}\int P\left(\frac{ct}{\sin(\theta)},a\right)dt = \lim_{\theta \to 0}\frac{c}{2a\sin(\theta)}\int_{-a}^{a}\frac{\sin(\theta)}{c}P(y,a)\,dy$$
$$= 1 \tag{4.4}$$

Thus, the area under the curve is unity, and the function approaches the $\delta$ function on boresight. Therefore, our E-plane expression is consistent with previous results on boresight.

In the H-plane, the proof is only a little more complicated. The field we calculated is

$$\bar{E}^{(h)}(r,t) = \bar{1}_y\left(\frac{-V}{r}\right)\frac{\cot(\theta)}{2\pi}\,\Phi^{(h)}\left(\frac{ct}{\sin(\theta)}\right) \tag{4.5}$$

Comparing this with (4.1), we find that for the two to be the same on boresight, it must also be true that

$$\delta_a(t) = \lim_{\theta \to 0} \frac{c \, f_g \cot(\theta)}{a} \, \Phi^{(h)}\!\left(\frac{ct}{\sin(\theta)}\right) \qquad (4.6)$$

where

$$\Phi^{(h)}(x) = \begin{cases} 1/(\pi f_g) \operatorname{arcsech}(-x/a) & -a \le x \le -a \operatorname{sech}(\pi f_g) \\ 1 & -a \operatorname{sech}(\pi f_g) \le x \le a \operatorname{sech}(\pi f_g) \\ 1/(\pi f_g) \operatorname{arcsech}(x/a) & a \operatorname{sech}(\pi f_g) \le x \le a \end{cases} \qquad (4.7)$$

Clearly the expression in (4.6) approaches infinity at $t = 0$. Next we check that the integral is equal to unity. Integrating (4.6), we find

$$\lim_{\theta \to 0} \frac{c \, f_g \cot(\theta)}{a} \int \Phi^{(h)}\!\left(\frac{ct}{\sin(\theta)}\right) dt = \lim_{\theta \to 0} \frac{c \, f_g \cot(\theta)}{a} \int_{-a}^{a} \frac{\sin(\theta)}{c} \Phi^{(h)}(x) \, dx$$

$$= \frac{f_g}{a} \int_{-a}^{a} \Phi^{(h)}(x) \, dx \qquad (4.8)$$

To carry out the integral, we need the result from Dwight[8, #738], that

$$\int \operatorname{arcsech}(x/a) \, dx = x \operatorname{arcsech}(x/a) + a \arcsin(x/a) , \quad [\operatorname{arcsech}(x/a) > 0] \qquad (4.9)$$

This leads to a final result for the integral of

$$\int_{-a}^{a} \Phi^{(h)}(x) \, dx = 2a \operatorname{sech}(\pi f_g) + \frac{2}{\pi f_g} \int_{a \operatorname{sech}(\pi f_g)}^{a} \operatorname{arcsech}(x/a) \, dx$$

$$= \frac{a}{f_g}\left(1 - \frac{2}{\pi} \arcsin(\operatorname{sech}(\pi f_g))\right) \qquad (4.10)$$

At high impedances $\operatorname{sech}(\pi f_g) \to 0$, so the second term in the above expression approaches 0. Combining this with (4.8), we find the area under the function is

$$\lim_{\theta \to 0} \frac{c \, f_g \cot(\theta)}{a} \int \Phi^{(h)}\!\left(\frac{ct}{\sin(\theta)}\right) dt = 1 \qquad (4.10)$$

This is the second condition required for the H-plane field to approach a $\delta$ function on boresight. Thus, the proof is complete and all our off-boresight fields are consistent with known results on boresight.

15

## V. Sample Field Calculations

Now that we are assured that the step responses are correct, we use them to plot some sample fields. To do so, we convolve the derivative of a typical driving voltage with the step response.

We use the integral of a Gaussian waveform to drive the antenna. Thus, the step response is convolved with a Gaussian waveform to get the actual radiated field. It is convenient to define the driving waveforms as

$$\frac{dv(t)}{dt} = \frac{V}{t_d} e^{-\pi(t/t_d)^2}, \qquad\qquad t_{FWHM} = 0.940\, t_d \qquad (5.1)$$

$$v(t) = \int_{-\infty}^{t} \frac{dv(t')}{dt'}\, dt', \qquad\qquad t_{10-90} = 1.023\, t_d \qquad (5.2)$$

where $t_{FWHM}$ is the Full Width Half Max of $dv/dt$, and $t_{10-90}$ is the 10-90% risetime of $v(t)$. These waveforms are plotted in Figure 8. Recall the definition of the derivative risetime of a waveform is

$$t_d = \frac{\max\,(v(t))}{\max\big(dv(t)/dt\big)} \qquad (5.3)$$

Thus, the derivative risetime is inversely proportional to the maximum derivative of the driving voltage. This is a useful property, since the peak of the radiated field is proportional to the peak of the derivative of the voltage. Note also that for the integrated Gaussian waveform shown above, the derivative risetime $t_d$ is within two percent of the 10-90% risetime, $t_{10-90}$.

The above expression for $v(t)$ can also be expressed in terms of the complementary error function. Thus,

$$v(t) = \begin{cases} V\Big[ \quad (1/2)\,\mathrm{erfc}(\sqrt{\pi}\,|t|/t_d)\Big] & t < 0 \\ V\Big[1 - (1/2)\,\mathrm{erfc}(\sqrt{\pi}\,t/t_d)\Big] & t \geq 0 \end{cases} \qquad (5.4)$$

where the complementary error function is defined in [11].

16

$$\frac{t_d}{V} \frac{dv(t)}{dt}$$

$t / t_d$

$$\frac{1}{V} v(t)$$

$t / t_d$

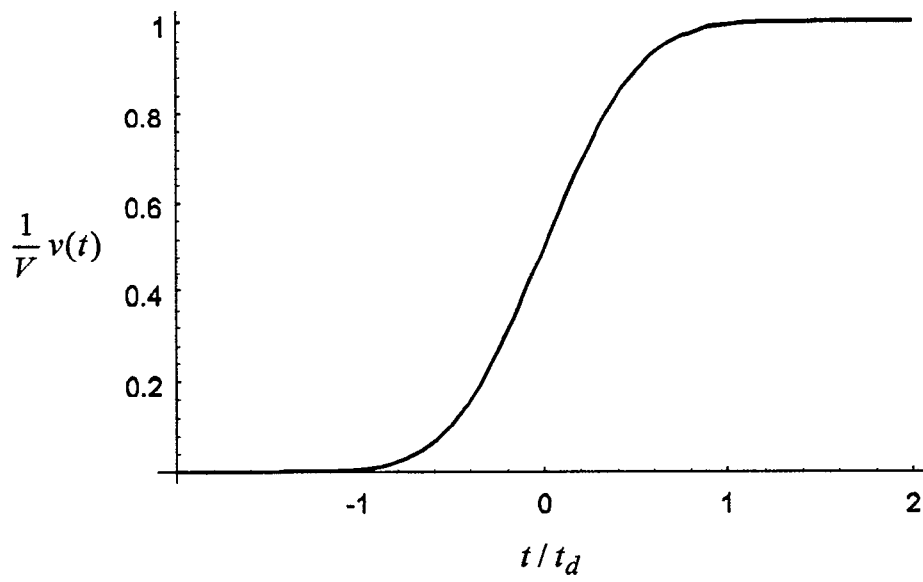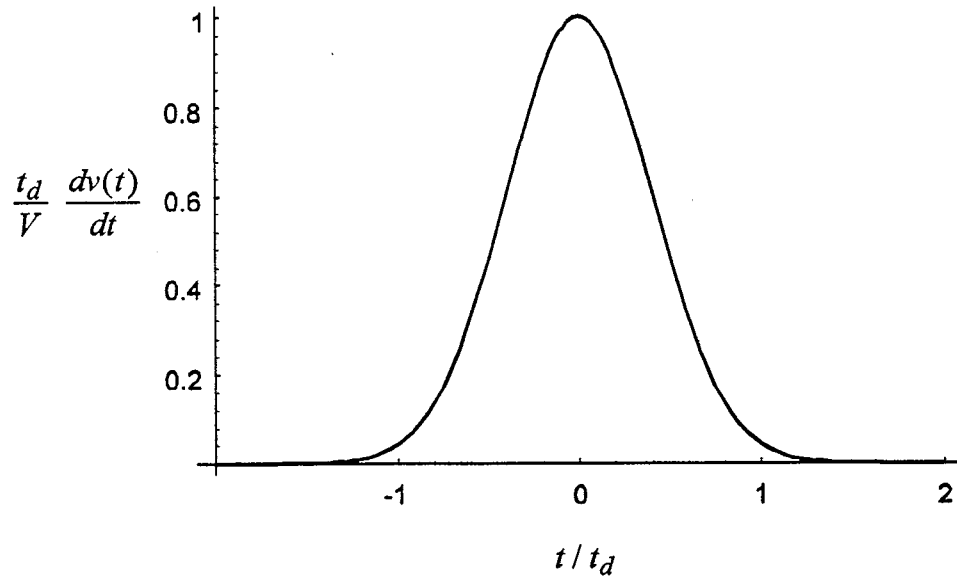Figure 8. Derivative of driving voltage (top), and its integral (bottom).

The radiated field is now calculated simply from

$$E(r,\theta,\phi,t) = \frac{1}{V}\frac{dv(t)}{dt} \circ E^{step}(r,\theta,\phi,t) \tag{5.5}$$

where the $\circ$ operator indicates a convolution, and $E^{step}(r,\theta,\phi,t)$ is the step response in the E- or H-plane, as calculated in Section III of this paper. We can reduce the number of cases that need to be calculated by defining a rise parameter

$$T_d = \frac{t_d}{t_a} = \frac{c\,t_d}{a} \tag{5.6}$$

All problems with equal rise parameters have the same shape radiated field. Thus, a field pattern is a function only of $T_d$, $f_g$, and $\theta$. There is no need to include a dependence upon both the aperture radius $a$ and the derivative risetime, $t_d$, because all the information is contained in $T_d$.

Let us now provide a typical example. Consider an IRA with a 400 $\Omega$ feed impedance and a radius of 0.3 m, driven by an integrated Gaussian voltage with $t_d = 250$ ps ($t_{10-90} = 256$ ns). For this configuration, $T_d = 0.25$, so all possible configurations with $T_d = 0.25$ and $Z_c = 400\,\Omega$ can be plotted on the same graph, with proper scaling. The fields in the E-plane and H-plane are shown in Figure 9. The time scale has to be normalized to either $t_a$ or $t_d$; it does not matter which. We have chosen to normalize to $t_a = a/c,$. For this configuration $t_a = 1$ ns, so it is trivial to normalize the $x$ axis.

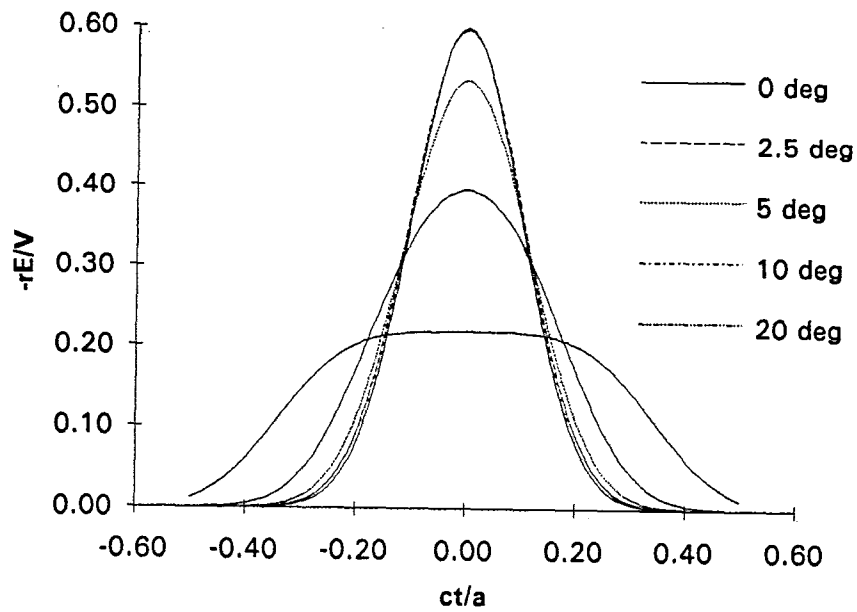With these results, we may now establish an antenna pattern. We do so in the section that follows.
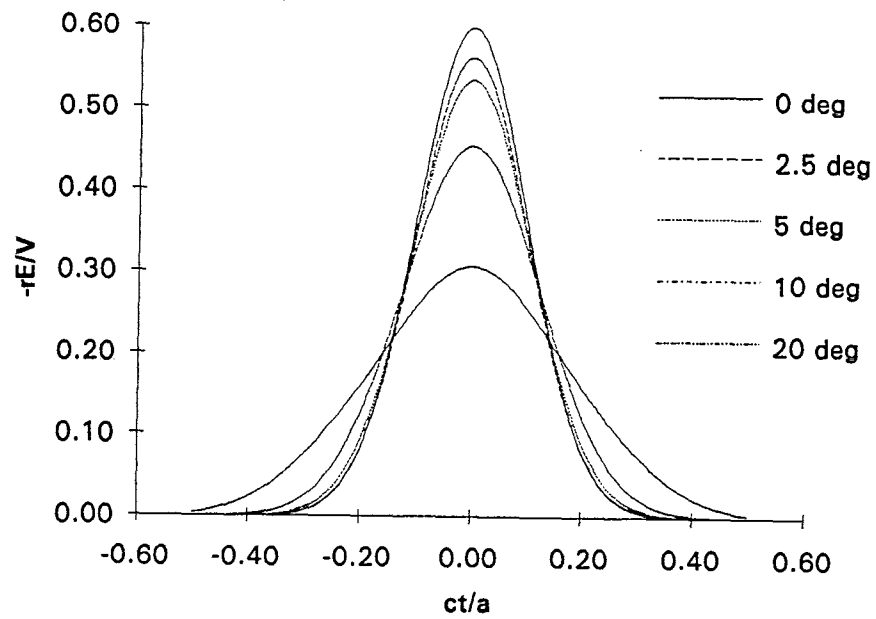
Figure 9. Radiated electric field vs. $\theta$ and $t$ in the H-plane (top) and E-plane (bottom) for $Z_c = 400\ \Omega$ and $T_d = 0.25$. Note that the curves in the E-plane at 0° and 2.5° nearly overlap.

## VI.  Antenna Pattern

With the off-boresight fields now calculated (at least approximately), we can establish the antenna pattern.  Recall from [4] the gain of an antenna in a particular direction for transmit mode is

$$G(\theta, \phi) \ = \ \frac{2 \pi c \sqrt{f_g} \left\| r E^{rad}(r, \theta, \phi, t) \right\|}{\left\| dV^{inc}(t)/dt \right\|} \tag{6.1}$$

It is simplest to think of the norm operator $\| \ \|$ as being the peak of the waveform ($\infty$–norm).  Of course, other interpretations are possible, such as the area under the curve (1-norm) or square root of power in the waveform (2-norm).  Recall the definition of an arbitrary $p$-norm

$$\left\| f(t) \right\|_p \ \equiv \ \left( \int_{-\infty}^{\infty} |f(t)|^p \, dt \right)^{1/p} , \qquad \left\| f(t) \right\|_{\infty} \equiv \sup_t |f(t)| \tag{6.2}$$

The norm one chooses must correspond to the experimental technique used in detecting the pulse.  Thus, when we use the peak norm ($\infty$–norm) in these calculations, we assume an experimental system that responds to the peak in the received waveform, as opposed to the power in the waveform (2-norm) or area in the waveform (1-norm).

The above gain definition may seem unusual at first, because it defines a gain with units of meters.  This definition, however, has a critical property that other definitions sometimes lack; i.e., it provides information about antenna performance in receive mode.  Thus, in receive mode, if the incident waveshape is a derivative of the driving voltage used in transmit mode (in this case a Gaussian), then the received voltage wave is described by

$$\left\| V^{rec}(t, \theta, \phi) \right\| \ = \ \sqrt{f_g} \; G(\theta, \phi) \left\| E^{inc}(\theta, \phi, t) \right\| \tag{6.3}$$

In other words, the peak received voltage is a simple function of the peak incident field.  Some other gain definitions do not offer such simple interpretations consistent with reciprocity.

We now plot the gain as a function of angle for the configuration of the previous section (Figure 10).  It is interesting to note that on boresight, the gain is just the aperture radius divided by $f_g^{1/2}$.  Furthermore, the pattern in the E-plane is somewhat more compressed than that in the H-plane.
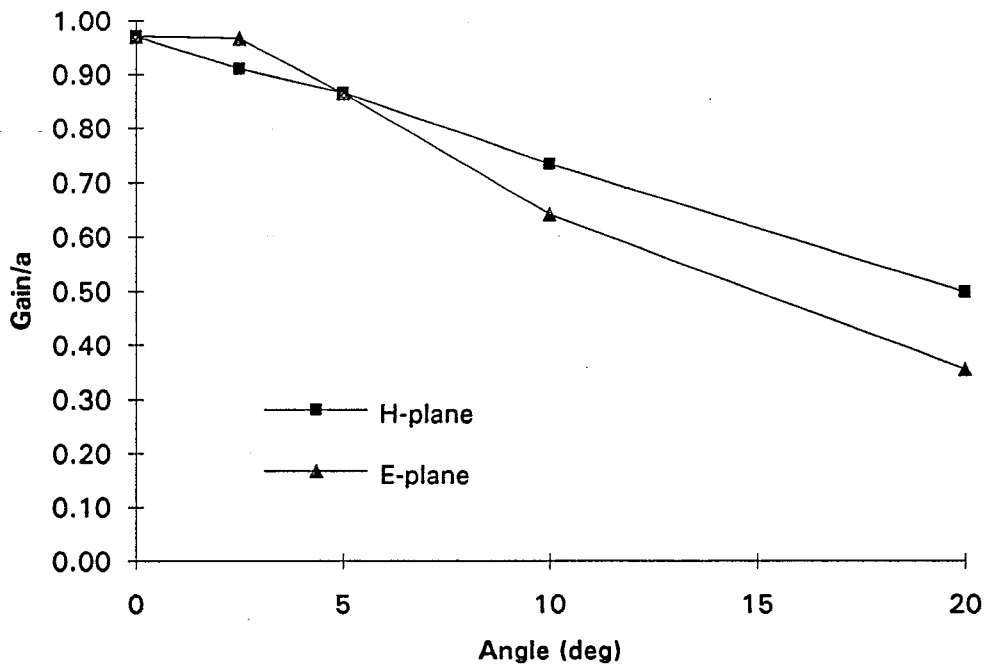
Figure 10. Gain ($\infty$-norm) in the H- and E-planes as a function of angle. For this plot, $Z_c = 400\ \Omega$, and $T_d = 0.25$ ($a = 0.3$ m and $t_d = 0.25$ ns).



Figure 11. Gain ($\infty$-norm) in the H- and E-planes as a function of angle. For this plot, $Z_c = 400\ \Omega$, and $T_d = 0.1$ ($a = 0.3$ m and $t_d = 0.1$ ns).

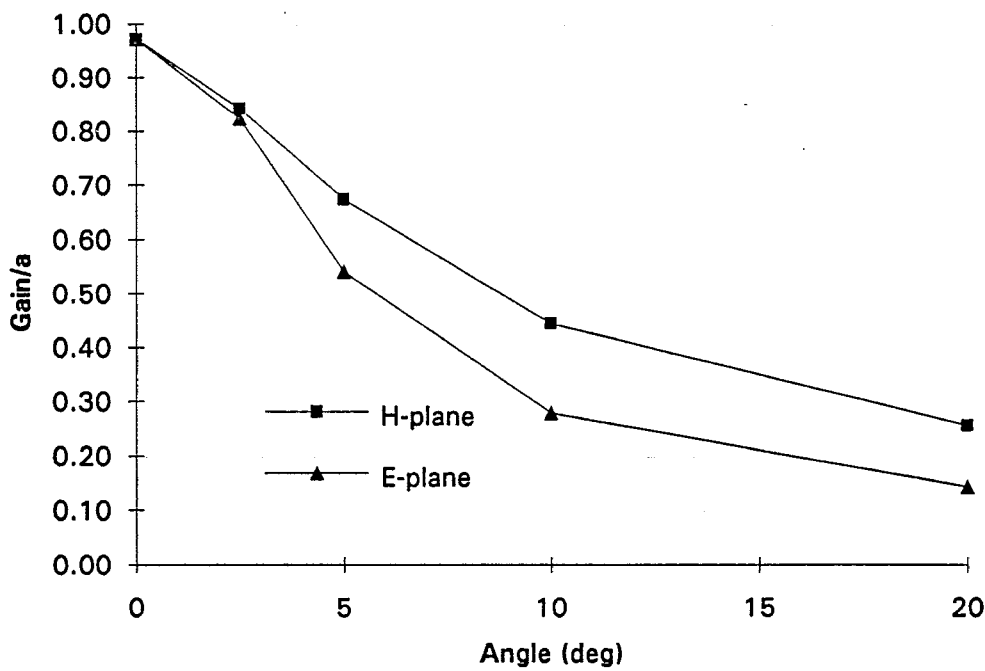The particular choice of parameters we have used until now has a slower rise parameter $T_d$ than what may be more typical. In order to see the difference, we plot the gain for a faster configuration, with $T_d = 0.1$ and the same feed impedance, $Z_c = 400 \ \Omega$. If we assume the same radius as before ($a = 0.3$ m), we have $t_d = 0.1$ ns., which is 2.5 times faster than the first case. The gain for this arrangement is shown in Figure 11. The overall effect is to make the patterns narrower. Also, we can see here more clearly that the E-plane pattern is narrower than the H-plane pattern.

It may be surprising, at first, to notice that the boresight gains of the two arrangements are the same. The faster configuration has a larger radiated field on boresight by a factor of 2.5, so one might think that the boresight gain must also be 2.5 times larger. But our definition of gain in (6.1) is such that the faster risetime appears in the denominator of (6.1) (the $dv/dt$ term), not in the gain. One could define a gain that included the factor of 2.5, but it's meaning in receive mode would then become less clear.

We can define a beamwidth as being the angular width where the pattern is down by a factor of two from its peak. Since this angular width depends upon the selection of the norm used in the gain definition, we call this beamwidth the Half Norm Beam Width (HNBW), analogous to the full-width half max (FWHM) beamwidth commonly used in the frequency domain. At higher $T_d$'s (larger apertures or faster risetimes) the beamwidth becomes narrower.

## VII. Discussion

There are a number of ways of controlling antenna pattern. Let us assume we have calculated a pattern, and we wish to make it broader. There are several ways of doing so.

The first technique for broadening pattern is to defocus the feed point of the aperture. Although this is conceptually simple, no simple models exist yet for predicting the effect. If one wanted to pursue this, one might use a technique similar to that used to predict TEM horn performance [12], which is another defocused aperture.

The second technique of broadening an antenna pattern is to use a smaller radius aperture. The third technique is to use a slower driving waveform (with a larger $t_d$). Both of these last two techniques increase the rise parameter $T_d$. In doing so, the on-boresight radiated field is reduced in inverse proportion to $T_d$. If one defocuses the antenna, the on-boresight radiated field is similarly reduced, but it is somewhat more difficult to predict the magnitude of this reduction.

The final technique for broadening an antenna pattern is to change the norm one is using to detect the signal. Recall that the norm one chooses in the gain definition must correspond to the experimental method of detecting the pulse. We have used the peak norm ($\infty$-norm) in this paper, however, both the 2-norm (power) and 1-norm (area) are reasonable choices. Furthermore, it can be shown that the 2-norm provides a broader pattern than the $\infty$-norm, and the 1-norm is broader still. Thus, if one is detecting a pulse using peak detection ($\infty$-norm), one could get a broader antenna pattern by detecting the power in the pulse (2-norm). One would get a broader pattern still by detecting the integral over the pulse (1-norm).

Conversely, if one wanted a narrower beam with a larger signal on boresight, one could use the opposite of these techniques. Thus, one would use large, well-focused apertures with fast risetimes (small $T_d$). Furthermore, one would detect the signal using peak detection ($\infty$-norm).

## VIII.  Conclusion

We have demonstrated a simple technique for calculating the early-time off-boresight radiated field generated by a reflector Impulse Radiating Antenna.  Aperture blockage is not included in the model, so the model is valid only at higher feed impedances.  This model leads to a simple interpretation of transient antenna gain, which we plot for some sample cases.  Because the models we developed are simple, one can readily understand how to control the antenna pattern by adjusting antenna parameters.

## References

[1]   C. E. Baum, Radiation of Impulse-Like Transient Fields, Sensor and Simulation Note 321, November 25, 1989.

[2]   C. E. Baum, Aperture Efficiencies for IRAs, Sensor and Simulation Note 328, June 24, 1991.

[3]   E. G. Farr, Optimizing the Feed Impedance of Impulse Radiating Antennas, Part I: Reflector IRAs, Sensor and Simulation Note 354, January 1993.

[4]   E. G. Farr and C. E. Baum, Extending the Definitions of Antenna Gain and Radiation Pattern Into the Time Domain, Sensor and Simulation Note 350, November 1992.

[5]   E. G. Farr and C. E. Baum, Prepulse Associated with the TEM Feed of an Impulse Radiating Antenna, Sensor and Simulation Note 337, March 1992.

[6]   W. R. Smythe, *Static and Dynamic Electricity*, third ed., New York: Hemisphere, 1989.

[7]   C. E. Baum and H. N. Kritikos, Symmetry in Electromagnetics, Physics Note 2, December 1990.

[8]   H. B. Dwight, *Tables of Integrals and Other Mathematical Data*, fourth ed., New York: Macmillan Publishing Co., 1961.

[9]   R. V. Churchill et al, *Complex Variables and Applications*, third ed., New York: McGraw-Hill, 1976.

[10]  C. E. Baum, Impedances and Field Distributions for Symmetrical Two Wire and Four Wire Transmission Line Simulators, Sensor and Simulation Note 27, October 10, 1966.

[11]  M. Abramowitz and I. A. Stegun, *Handbook of Mathematical Functions*, National Bureau of Standards, December 1972

[12]  E. G. Farr and C. E. Baum, A Simple Model of Small-Angle TEM Horns, Sensor and Simulation Note 340, May 1992.